Applied Catalysis B: Environmental 238 (2018) 609–617

Contents lists available at ScienceDirect

Applied Catalysis B: Environmental

journal homepage: www.elsevier.com/locate/apcatb

Platinum and N-doped carbon nanostructures as catalysts in hydrodechlorination reactions

C. Ruiz-García, F. Heras*, L. Calvo, N. Alonso-Morales, J.J. Rodriguez, M.A. Gilarranz

Chemical Engineering Section, Faculty of Science, Universidad Autónoma de Madrid (UAM), Cantoblanco, 28049 Madrid, Spain

ARTICLE INFO

Keywords:
Hydrodechlorination
Water treatment
Pt nanoparticles
Mesoporous carbon
Doped carbon

ABSTRACT

Novel Pt catalysts supported on undoped and N-doped (1% N, w) carbons with well interconnected and nanostructured mesoporosity ($V_{mesopore}$ = 0.65 $cm^3\,g^{-1}$, S_{EXT} = 730 $m^2\,g^{-1}$) were prepared and tested in the hydrodechlorination of 4-chlorophenol in water at 30–70 °C. The growth of Pt nanoparticles was achieved using incipient wetness impregnation and a modified colloidal synthesis. Total conversion of 4chlorophenol and 100% selectivity to cyclohexanol was achieved. The remarkable activity in the hydrogenation of the phenol resulting from hydrodechlorination has not been reported before with Pt catalysts and it is of high interest because it maximizes detoxification. When the Pt NPs were synthesized by incipient wetness impregnation some influence of the N-doping of the support was observed in the size and electronic state of the NPs. However, highly reproducible Pt NPs were prepared by in situ colloidal synthesis regardless the nature of the support. In this last case similar activity was observed for the catalysts with undoped and N-doped carbon support, although the activity increased more with temperature for the later. Apparent activation energies of 15–25 kJ mol^{-1} were obtained for the disappearance of 4-chlorophenol.

1. Introduction

There are many nanostructures which can adopt a huge number of configurations and play a relevant role as catalysts and catalytic supports in the development of new strategies in the field of catalysis. The carbon nanostructures constitute a remarkable and expanding group. From the point of view of catalysis the possibility of designing and preparing nanostructured carbon materials with controlled pore texture hosting metallic nanoparticles in their pores is of great interest.

It has been shown that reproducible nanostructured carbons can be prepared by the template technique, which allows obtaining materials with a controlled porosity and morphology as the patterned inverse replica of a selected mold [1,2]. SBA15, MCM-41 or MSU-F are mesoporous silicas commonly used as templates or molds to obtain a wide variety of nanostructured carbons. These carbon materials may host metallic nanoparticles within optimum porous structure for catalysis [3]. Thus, the regular mesoporosity achievable reduces the mass transfer constraints due to small pore size and increases the exposure of the active phase to the reactants [4,5]. The width of the pores hosting the metallic phase can also affect to the activity and selectivity of the catalysts, the adsorption steps and the activation energies [6–8].

The literature describes examples of the preparation of a variety of nanostructures and their use as catalysts in various reactions. For instance, the Suzuki coupling using Pd confined in a mesoporous silica, the reduction of 4nitrophenol with a Pt catalyst within yolk/shell structure or the detoxification of water by hydrodechlorination using Pd supported on mesoporous carbon [9].

Carbon materials have been used as catalysts or catalyst supports due to their high thermal and chemical stability and potential role in the reaction pathway. Thus, the versatility of carbon-based materials also lies on the possibility of modifying their chemical structure by functionalization and doping, among other techniques. Doping induces changes in the electrical and chemical properties that depend on the heteroatom inserted, being the most commonly used oxygen, sulfur, phosphorus, nitrogen and boron. The usefulness of carbon doping has been shown in catalysis and adsorption [3,9,10]. Nitrogen is the most frequent doping element due to its atomic similarity with carbon, and the n-type modifications achieved.

This work focuses on the synthesis of catalysts based on nanostructured carbons prepared using SBA-15 as template and with a chemical composition modified by doping with nitrogen. These carbon materials were used to host platinum nanoparticles by incipient wet impregnation and by a modified colloidal method [11,12] that provides additional control of the size, stability and exposure of the Pt phase to the reagents. The Pt/C nanostructured catalysts are expected to show diminished mass transfer limitations, thus achieving high activity and

* Corresponding author.
E-mail address: fran.heras@uam.es (F. Heras).

https://doi.org/10.1016/j.apcatb.2018.07.054
Received 5 February 2018; Received in revised form 12 July 2018; Accepted 18 July 2018
Available online 23 July 2018
0926-3373/ © 2018 Elsevier B.V. All rights reserved.

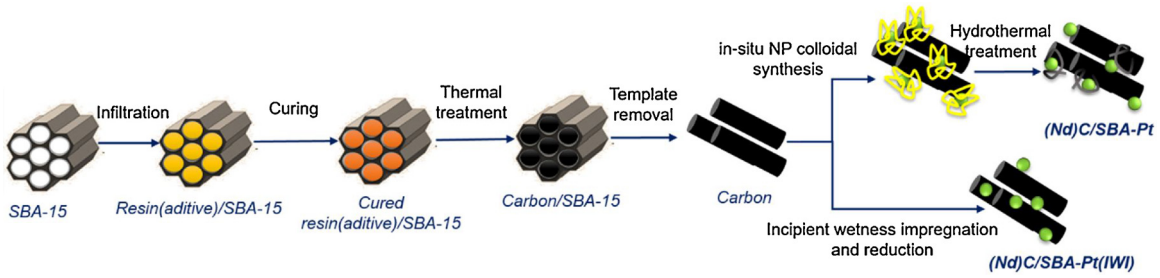

Fig. 1. Synthetic route for the preparation of catalysts.

enabling to study the interaction between the active phase and the N-doped carbon. The catalysts have been tested in the hydrodechlorination (HDC) of 4-chlorophenol. HDC has been recognized as a potential detoxification technology in wastewater treatment, and it has been found that the activity of metallic catalysts in this reaction is very sensitive to the chemical composition of the support and the structure of the metallic phase [13,14].

2. Experimental

2.1. Preparation of nanostructured carbon supports and catalysts

Fig. 1 shows the steps in the preparation of the templated nanostructured carbon supports and the catalysts. In a typical preparation of a templated carbon 1 g of resol resin (Bakelite®PF9934 FL, Hexion Specialty Chemicals Ibérica S.A.) and 1 g of SBA-15 (mesostructured, SiO_2 99%, Sigma-Aldrich) template were used. In the case of N-doped carbon, 0.10 g of 1,10phenantroline (99%, Sigma-Aldrich) were also added to the resin. These precursor materials were mixed using 100 mL of ethanol (99.8%, Sigma-Aldrich) and then infiltrated in the SBA-15 in a rotatory vacuum evaporator at 100 mbar and 40 °C until dryness. Then, the resin was cured by heating the sample at 135 °C for 1 h in air atmosphere. The cured resin-silica was treated at 700 °C for 1 h, using a temperature ramp of 5 °C min^{-1}, in N_2 flow (50 N mL min^{-1}). The silica template was removed by washing with 3.5 M NaOH solution for 15 h and the remaining solid was filtered (0.45 µm Nylon filter), washed with water until neutral pH and oven-dried at 65 °C. The undoped and N-doped carbons were denoted as C/SBA and NdC/SBA, respectively.

Pt nanoparticles were synthesized on the templated carbons using the original in situ colloidal synthesis method previously described by Lemus et al [11]. In a typical synthesis 52 mg of $H_2PtCl_6{\cdot}6H_2O$ (ACS reagent. ≥37.50% Pt basis), 0.3 mL of 0.2 N HCl (Sigma Aldrich, 37%) and 50 mL of distilled water were mixed in order to obtain a stock solution, which was mixed with 0.65 g of carbon and stirred for 30 min. Polyvinylpyrrolidone (PVP, average mol. wt. 40.0 g mol^{-1}, Sigma-Aldrich) was added to the solution under stirring until a PVP/Pt molar ratio of 10 was achieved, and finally 5 mL of $NaBH_4$ were added dropwise up to a $NaBH_4$/Pt molar ratio of 10 to reduce the Pt precursor. An additional stirring time of 30 min was provided and the resulting reaction mixture was evaporated in a rotary vacuum evaporator at 100 mbar and 60 °C until dryness. Then, the catalysts were subjected to hydrothermal treatment to remove PVP in a magnetically stirred three-necked steel reactor (Berghof. model BR100). In a typical treatment, 20 mL of water were placed in the reactor together with 100 mg of catalyst and heated at a rate of 3 °C min^{-1}–200 °C and 17 bar under stirring for 4 h. After cooling to room temperature, the material was separated from the aqueous phase by filtration (0.45 µm Nylon filter) and dried at 60 °C. Additionally, some catalysts were prepared from the templated carbons by incipient wetness impregnation (3% Pt, carbon basis). The templated carbon supports were impregnated with $H_2PtCl_6{\cdot}6H_2O$, using a solution volume that was 1.3 times the pore volume of the support. The impregnated solid was dried at 65 °C overnight, calcined at 200 °C for 2 h and reduced at 200 °C in H_2 atmosphere. The catalysts with nanoparticles prepared by in situ colloidal synthesis were denoted as C/SBA-Pt and NdC/SBA-Pt, whereas those prepared by incipient wetness impregnation were denoted as C/SBA-Pt(IWI) and NdC/SBA-Pt(IWI).

2.2. Materials characterization

Bulk chemical elemental analyses were performed in a LECO CHNS-932 equipment. Pore texture was studied from the nitrogen adsorption-desorption isotherms obtained in a Tristar II 3020 apparatus (micromeritics). Samples were degassed at 130 °C for at least 4 h under vacuum (~0.1 mbar). The surface area was calculated by the Brunauer–Emmet–Teller (BET) equation, external surface and micropore volume were obtained from the t-plot and the Barrett-Joyner-Halenda (BJH) method was used to calculate the mesopore volume and mean diameter. The morphology of the carbons and metal nanoparticles was studied by transmission electron microscopy (TEM) with a JEM 2100 microscope. The size of the Pt nanoparticles was calculated from measurements made with J-image program and considering at least 200 nanoparticles from different TEM images. The electronic state of Pt and N elements was determined by X-ray photoelectron spectroscopy (XPS) using a K-Alpha-Thermo Scientific spectrometer with monochromatic Al Kα radiation (12 kV, 6 mA), a pass energy of 40 eV, energy step size of 0.1 eV and 300 scans for Pt 4f and 150 for N 1s. The binding energies of the spectra were corrected using the C 1s peak at 284.6 eV as standard [15].

2.3. Hydrodechlorination experiments

The catalysts were tested in the aqueous phase hydrodechlorination (HDC) of 4-chlorophenol (4-CP), which was selected as target compound to facilitate comparison of the results with those in the literature. This reaction gives as possible products phenol, cyclohexanone and cyclohexanol [16,17].

The HDC experiments were carried out in a glass batch stirred reactor using 0.150 L of a 0.1 g L^{-1} 4-CP aqueous solution, a Pt concentration of 2.4–10.0 mg L^{-1}, continuous 50 N mL min^{-1} hydrogen flow, constant stirring at 800 rpm, ambient pressure and controlled temperature covering the 30–70 °C testing range. Samples were collected at regular intervals of time amounting a total withdrawn volume lower than 10% of the initial volume. The samples were filtered and analyzed by HPLC (Prostar, Varian), using a C18 column at 40 °C, to determine 4-CP and phenol concentration, whereas cyclohexanone and cyclohexanol concentrations were measured by GC-FID (GC 3900 Varian) with a capillary column (CP-Wax 52 CB. Varian) and N_2 as carrier gas.

The experimental data of 4-CP disappearance were fitted to a pseudo-first order rate equation:

$$C_{4-CP} = C_{4-CP_0} e^{kt}$$

The specific activity (a) of the catalysts was calculated from the pseudo-first order rate constant (k) according to:

Table 1
Elemental analyses of the templated carbons and catalysts.

Sample	Bulk chemical elemental analysis				Elemental analysis by XPS				
	C (% w)	H	N	N/C (w/w)	C (% w)	O	N	Pt	N/C (w/w)
C/SBA	86.5	2.1	0.1	0.001					
NdC/SBA	84.6	2.1	0.7	0.009					
C/SBA-Pt	68.8	1.7	0.6	0.009	83.7	7.3	2.2	2.2	0.026
NdC/SBA-Pt	72.4	2.1	0.8	0.011	78.4	14.1	0.7	2.1	0.009
C/SBA-Pt(IWI)					93.8	3.0	0.3	2.8	0.003
NdC/SBA-Pt(IWI)					86.7	6.0	0.5	4.7	0.006

$$a\left(\frac{mmol}{g\ Pt \cdot min}\right) = k \cdot \frac{C_{4-CP_0}}{C_{Pt}}$$

Where $C_{4\text{-}CPo}$ is the initial concentration of 4-CP and C_{Pt} is the concentration of Pt. The apparent activation energy was calculated using the Arrhenius's equation

$$k = k_0 \cdot e^{\frac{-Ea}{RT}}$$

The selectivity for a given reaction time was calculated as mol of reaction product per mol of 4-CP converted.

3. Results and discussion

3.1. Characterization

The bulk elemental analyses (Table 1), show that the undoped templated carbon (C/SBA) presents a N content of 0.1% w, probably due to some additives included in the commercial resin formulation. In the case of the templated N-doped carbons prepared adding 1,10-phenantroline as doping agent (NdC/SBA) a N content of 0.7% (w) was achieved, corresponding to a N/C weight ratio of 0.009. Thus, supports representative of undoped and N-doped carbon were successfully obtained. Regarding the bulk elemental analyses of the catalysts, it should be noted that the incorporation of the Pt-PVP NPs and the further hydrothermal treatment for the removal of PVP leads to an increase in the bulk nitrogen content of C/SBA-Pt catalyst from 0.1 to 0.7% (w). This is related to PVP fragments remaining on the carbons and seems to be favored for the undoped support, since the increase in nitrogen content in the case of NdC/SBA-Pt is of low significance.

The XPS spectra of N 1s region (Fig. 2) show different N contributions on the surface of the catalysts. The bands corresponding to pyrrolic and to imine, amide or amine groups, are centered around 400.3–400.5 and 399.6–399.7 eV. These signals can be appreciated in the spectra of C/SBA-Pt and NdC/SBA-Pt and can be ascribed to the PVP used in the colloidal synthesis of Pt NPs, since the C/SBA support was not doped with nitrogen. In the case of NdC/SBA-Pt, a third contribution centered around 398.4–398.6 eV and ascribable to pyridinic nitrogen can be observed. The main part of the pyrrolic and all the pyridinic species can be attributed to the doping process, since these are the main contributions in the doped carbon NdC/SBA and for this sample the only source of nitrogen was the doping agent.

The elemental analyses from the XPS spectra (Table 1) show higher values of nitrogen content than the bulk chemical elemental analyses, which indicates that nitrogen is more concentrated at the external surface or the catalysts. This is particularly evident in the case of C/SBA-Pt, showing that remaining PVP and PVP fragments are more concentrated at the external surface of the catalyst particles.

The nanostructuration of the templated carbons can be deduced from the TEM micrographs shown in Fig. 3. Carbon rods are formed due to filling of cylindrical pores of SBA-15 by resol resin and further pyrolysis. The high pyrolysis yield of the resin (ca. 70%) contributes to the formation of well-defined rods. After the removal of the template, the

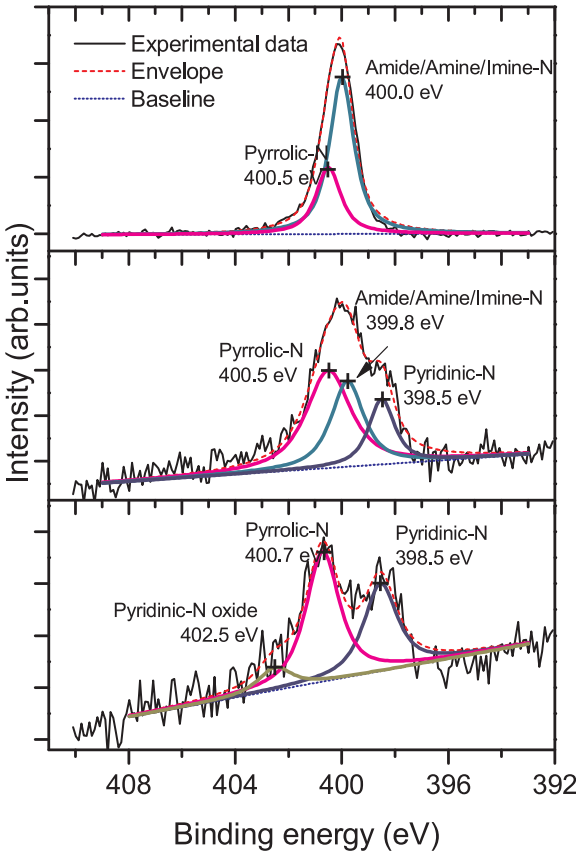

Fig. 2. XPS of N 1s of the catalysts A) C/SBA-Pt, B) NdC/SBA-Pt; and C) N-doped carbon support NdC/SBA.

void spaces generated among the rods are responsible for the pore volume of the templated carbons, thus a good pore connectivity was achieved. It can also be observed that the particles of templated carbon consist of arrangements of cylindrical rods resembling the shape of the starting SBA-15 particles (Figs. 3 and S1).

The 77 K nitrogen adsorption-desorption isotherms (Fig. 4) of the nanostructured templated carbons reveal a significant contribution of micro and mesoporosity with a hysteresis cycle of H1 type, according to IUPAC classification [18]. The materials synthesized in this work show a high contribution of mesoporosity, due to the silica walls in the template, intersections of slits, and also probably because the filling of the SBA-15 cylindrical pores with the resin is not complete in all cases and there may be some void spaces within the rod arrangements [19]. On the other hand, the significant micropore contribution could be related with the removal of heteroatoms from the precursor upon carbonization, which is particularly evident in the case of NdC/SBA due to the larger nitrogen content of the precursor mixture. The external or non-microporous surface area shows equivalent values for undoped and

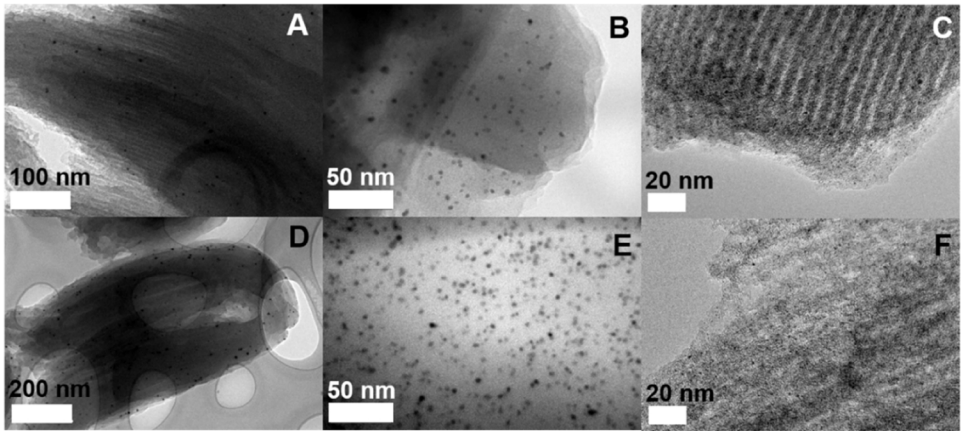

Fig. 3. TEM micrographies of the carbon particles A–B) NdC/SBA-Pt, C) NdC/SBA-Pt(IWI), D–E) C/SBA-Pt, and F) C/SBA-Pt(IWI).

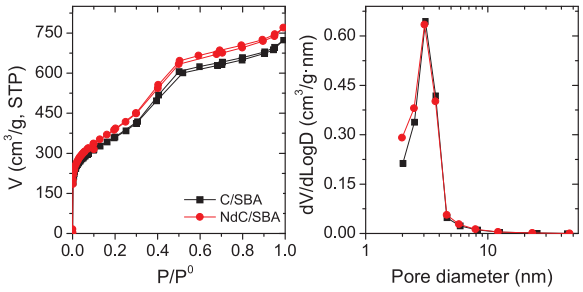

Fig. 4. 77 K N_2 adsorption-desorption isotherm of the nanostructured templated carbons and pore width distribution.

Table 2
Porous texture of the nanostructured templated carbons.

Sample	S_{BET} (m^2/g)	S_{EXT}	V_{meso} (cm^3/g)	V_{micro}	$\bar{d}_{pore}$ (nm)
C/SBA	1273	730	0.645	0.396	3.44
NdC/SBA	1390	722	0.653	0.467	3.34
C/SBA(IWI)	1387	710	0.662	0.448	3.57
NdC/SBA(IWI)	1018	743	0.664	0.307	3.68

N-doped templated carbons, with remarkable values of 722–730 m^2/g (Table 2) and pore size centered at 3.4 nm. Therefore, the materials obtained are nanostructured carbons with equivalent morphology and porous texture in the mesopore range, only differing in the chemical composition of the carbon matrix. The differences in micropore contribution can be neglected for the aims of this work, i.e. the use of the materials as supports of catalysts to be tested in aqueous phase.

The representative TEM images of the catalyst prepared by colloidal method shown in Fig. 3 evidence that the Pt NPs have a homogeneous distribution on the support, regardless the carbon is undoped or N-doped. Likewise, a mean NP size around 3.9 ± 1.5 nm and 3.6 ± 1.1 nm was calculated for C/SBA-Pt and NdC/SBA-Pt, respectively, from the histograms shown in Fig. 5. This indicates that the synthesis method of Pt NPs and the assembly on different carbons (undoped and N-doped) leads to reproducible metallic phase size and dispersion. The formation of equivalent metallic phase for both carbons is also supported by the XPS spectra of the Pt 4f region (Fig. 6), which show nearly identical distribution of Pt species, with Pt^{n+}/Pt° ratios of 1.0. It is important to remark that the amount of Pt available on the surface of the catalyst is the same for both carbon supports, as it can be seen in Table 1. On the contrary, when the Pt NPs were prepared by IWI some differences were detected between the catalysts with undoped and N-doped support. The histograms in Fig. 5 show smaller Pt NPs for

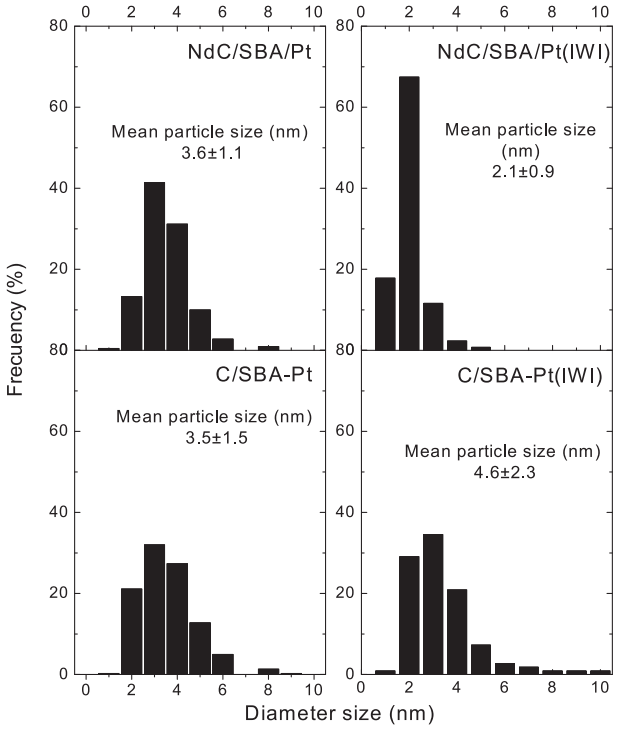

Fig. 5. Pt NP size distribution for the catalysts studied.

NdC/SBA-Pt(IWI) (2.1 ± 0.9 nm) than for C/SBA-Pt(IWI) (4.6 ± 2.3 nm). The support also affects to the distribution of Pt species. While the Pt^{n+}/Pt° ratio yields a value of 0.5 for C/SBA-Pt(IWI) it increases to 1.2 for NdC/SBA-Pt(IWI) (Fig. 6). Therefore, in the synthesis by IWI the support influences the structure of the metal phase, whereas in the in situ colloidal synthesis PVP seems to shield the carbon surface thus diminishing the influence of the support on NPs growth.

3.2. Hydrodechlorination results

Preliminary HDC experiments were carried out using different concentrations of metal in the reaction medium. The evolution of the concentration of 4-CP and reaction products in the runs carried out with a concentration of Pt between 2.4 and 10.0 mg L^{-1} can be seen in Fig. 7 for NdC/SBA-Pt and C/SBA-Pt catalysts. The kinetic constant obtained by fitting the data to a pseudo-first order rate equation was used to calculate the specific catalytic activity (Pt mass-normalized) of the catalysts (Table 3). Fig. 8 shows that at the lowest Pt concentration slightly lower activity values were obtained. Similar values of Pt

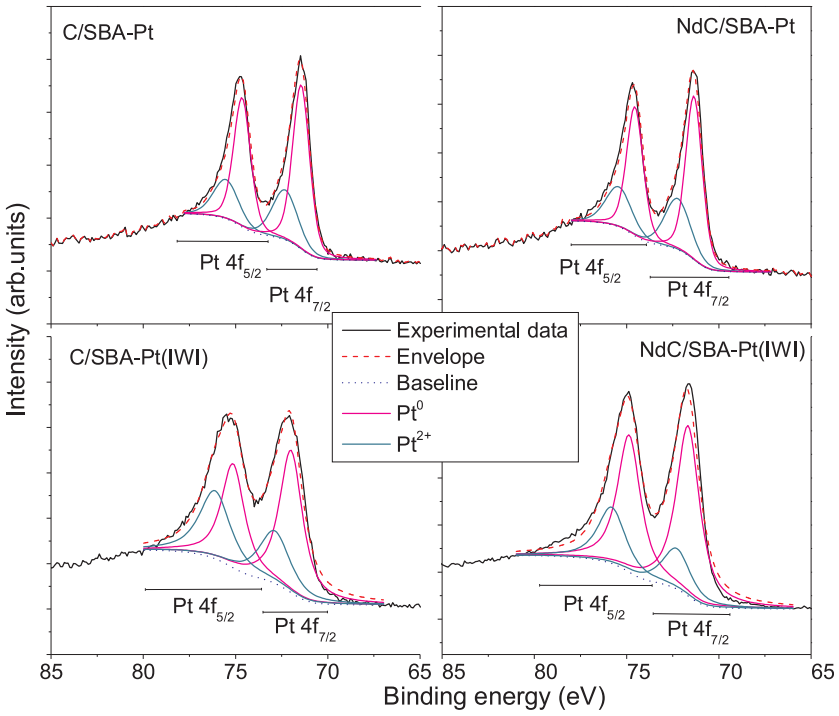

Fig. 6. Deconvolution of Pt 4f XPS bands for the catalysts studied.

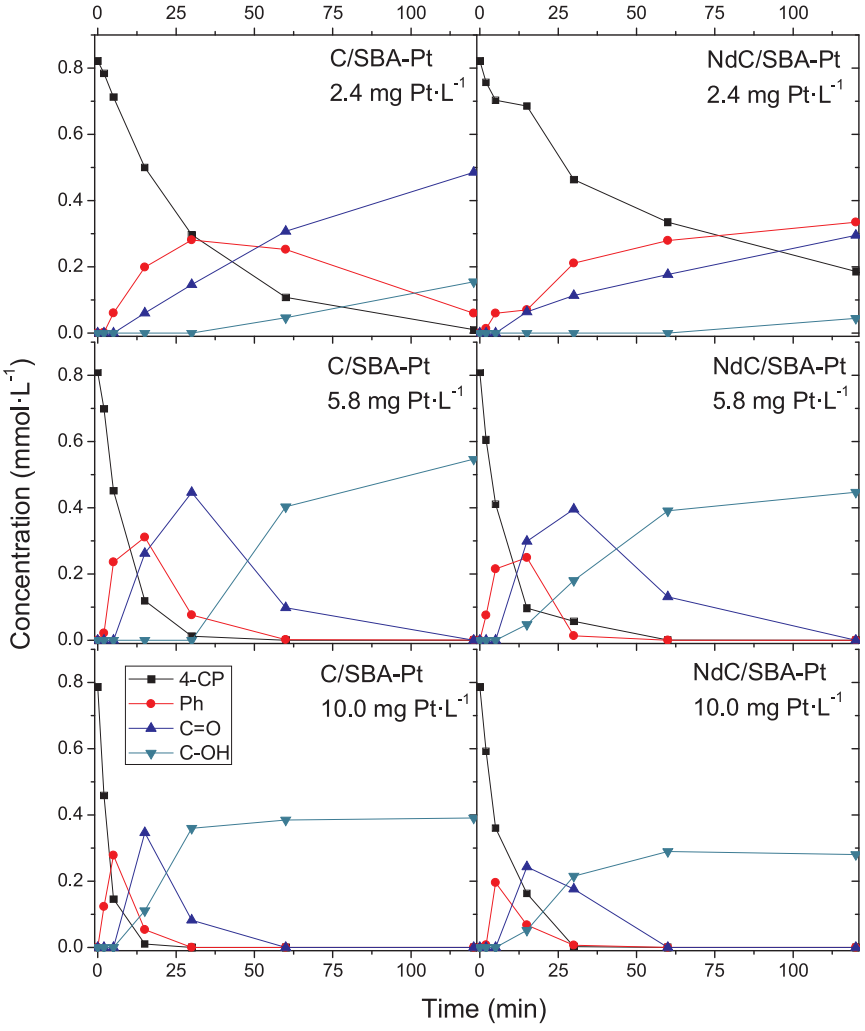

Fig. 7. Time course of 4-CP (■), phenol (●) and cyclohexanone (▲) and cychlohexanol (▼) concentration in the HDC experiments (2.4–10 mg $Pt{\cdot}L^{-1}$, $[4\text{-CP}]_0 = 100\ mg L^{-1}$, T = 30 °C).

Table 3
Selectivity and kinetic parameters obtained in the HDC runs with NdC/SBA-Pt and C/SBA-Pt catalysts at 30 °C.

C_{Pt} (mg Pt·L^{-1})	Sample	4-CP conversion (%)[1]	Selectivity[a] (%)[a]			$k_{4\text{-CP}}$ (min^{-1})	R^2	a (mmol·gPt^{-1}·min^{-1})
			Ph	C = O	C-OH			
2.4	C/SBA-Pt	99	0	0.34	0.66	0.039	0.999	14
	NdC/SBA-Pt	77	0.28	0.58	0.14	0.017	0.980	6
5.8	C/SBA-Pt	100	0	0	1.0	0.146	0.997	20
	NdC/SBA-Pt	100	0	0	1.0	0.120	0.999	17
10.0	C/SBA-Pt	100	0	0	1.0	0.258	0.995	20
	NdC/SBA-Pt	100	0	0	1.0	0.181	0.999	14

[a] 120 min reaction time.

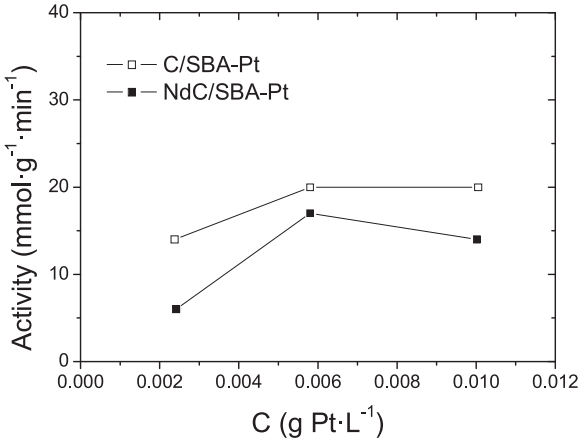

Fig. 8. Activity of NdC/SBA-Pt and C/SBA-Pt catalysts at different metal concentration in the reaction media.

specific activity were obtained for metal concentrations of 5.8 and 10.0 mg L^{-1} in the case of NdC/SBA-Pt, whereas a decline of low significance was observed for C/SBA-Pt. Therefore, the low influence of metal concentration in the specific activity indicates minor or negligible mass transfer constrains.

From Fig. 7 it can also be seen that both NdC/SBA-Pt and C/SBA-Pt enabled complete disappearance of 4-CP within the whole range of Pt concentration. The occurrence of phenol, cyclohexanone and cyclohexanol indicates a typical scheme of consecutive reactions [16,17]. This distribution of reaction products supports a reaction pathway where the primary product of 4-CP HDC is essentially phenol, which is then hydrogenated to cyclohexanone, and this last to cyclohexanol. In the experiments with a high metal concentration a remarkable activity of the catalysts in the hydrogenation of phenol and cyclohexanone can be observed. When the concentration of metal was increased to 5.8 and 10.0 mg Pt·L^{-1} the reaction rate was higher with both catalysts and cyclohexanol became the only product in the reaction medium after 60–120 min of reaction time.

The main differences can be observed at the lowest concentration of catalyst (2.4 mg Pt·L^{-1}), where NdC/SBA-Pt exhibited higher hydrogenation activity. Platinum has not received the same attention as Pd or Rh in HDC studies, mainly due to its lower stability and activity. Previous works on the use of Pt catalysts supported on pillared clays reported phenol as the only product from 4-CP HDC and low activity in comparison to Pd [20,21]. However, Munoz et al. [22] reported an improved activity in 4-CP HDC and hydrogenation of phenol using bimetallic Pt-Ce and Pt-Ni catalysts. Lower 4-CP conversion and hydrogenation was also observed for Pt-Al_2O_3 catalysts [23]. To the best of our knowledge, no other Pt catalyst in the literature has been reported to achieve complete HDC of 4-CP and total hydrogenation to cyclohexanol. This feature of the catalyst here presented is relevant, since total selectivity to cyclohexanol implies maximum removal of toxicity [24].

The NdC/SBA-Pt and C/SBA-Pt catalysts were also evaluated in the HDC of 4-CP at three different temperatures, in the 30–70 °C range, using a Pt concentration of 5.8 mg Pt·L^{-1} (Fig. 9), to study more in depth the effect of doping the support. In all cases total conversion of both 4-CP and phenol was observed after a reaction time of 120 min. With all the catalysts, the selectivity to cyclohexanone increased for the reactions at 50 and 70 °C. Likewise, the occurrence of cyclohexanol took place from shorter reaction time with NdC/SBA-Pt, which can be attributed to nitrogen doping of the support.

The activity values (Table 4) were very close for NdC/SBA-Pt and C/SBA-Pt at 30 and 50 °C, with slightly higher activity for C/SBA-Pt. However, at 70 °C the most active catalyst was NdC/SBA-Pt, indicating some influence of support doping. The activation energy was calculated for NdC/SBA-Pt and C/SBA-Pt catalysts in the 30–70 °C range from the kinetic constants obtained by fitting the data to a pseudo-first order rate equation for 4-CP disappearance. The values obtained for both catalyst were relatively close, 23 ± 5 and 15 ± 2 kJ·mol^{-1} for the catalyst with undoped and N-doped support, respectively. Diaz et al. also reported some influence of the support in the activation energy for the HDC of 4-CP with Pt catalysts, with values of 26.2 kJ·mol^{-1} for Al_2O_3-[23] and 58.2 kJ·mol^{-1} for activated carbon-supported [16] catalysts. The values obtained in the current work are in the lower range, and even below, reported in literature for a diversity of catalysts tested in the HDC of 4CP (21.7–61.5 kJ·mol^{-1}) [16,17,20,25–30]. Our low values could be indicative of some contribution of physical phenomena to the overall reaction rate, which was also assessed using the results of additional experiments and the Carberry and Weisz-Prater parameters (Supplementary material), although the values estimated for these parameters indicated a minor contribution of such phenomena. Interestingly, Munoz et al. reported an activation energy of 15.0 kJ·mol^{-1} for the adsorption of 4-CP on Pd/C catalysts and a relevant contribution of adsorption to the overall HDC process rate [17,30,31] during hydrodechlorination reactions. In other hydrogenation reactions catalyzed with Pt NPs, the apparent activation energy decreased to values of 12–18 kJ·mol^{-1} as a consequence of the optimization of the catalyst activity, which may be related to a change in the control regime, even though no mass transfer limitations were observed [32,33].

Some additional experiments were carried out using the catalyst prepared by incipient wetness impregnation in order to study the crossed effect of support doping and the method used for the synthesis of Pt NPs (Fig. 10). The activity value obtained (Table 5) for the C/SBA-Pt(IWI) catalyst was 17 mmol·g^{-1} Pt·min^{-1}, which is lower than for C/SBAPt (27 mmol·g^{-1} Pt·min^{-1}). The activity for NdC/SBA-Pt(IWI) catalyst was 25 mmol·g^{-1} Pt·min^{-1}, identical to that obtained for NdC/SBA-Pt. The higher activity obtained for the catalyst prepared by incipient wetness impregnation with N-doped support can be related to a better dispersion of Pt NPs (lower mean nanoparticle size: 2.1 nm) and the higher Pt^{n+}/Pt° ratio. In contrast, when the Pt NPs were synthesized in the PVP environment, i.e. with lower interaction with the support during the growth of Pt NPs, the doping of the support did not lead to relevant changes of activity within the 30–50 °C range. Therefore, for the catalysts prepared by incipient wet impregnation the N-doping of

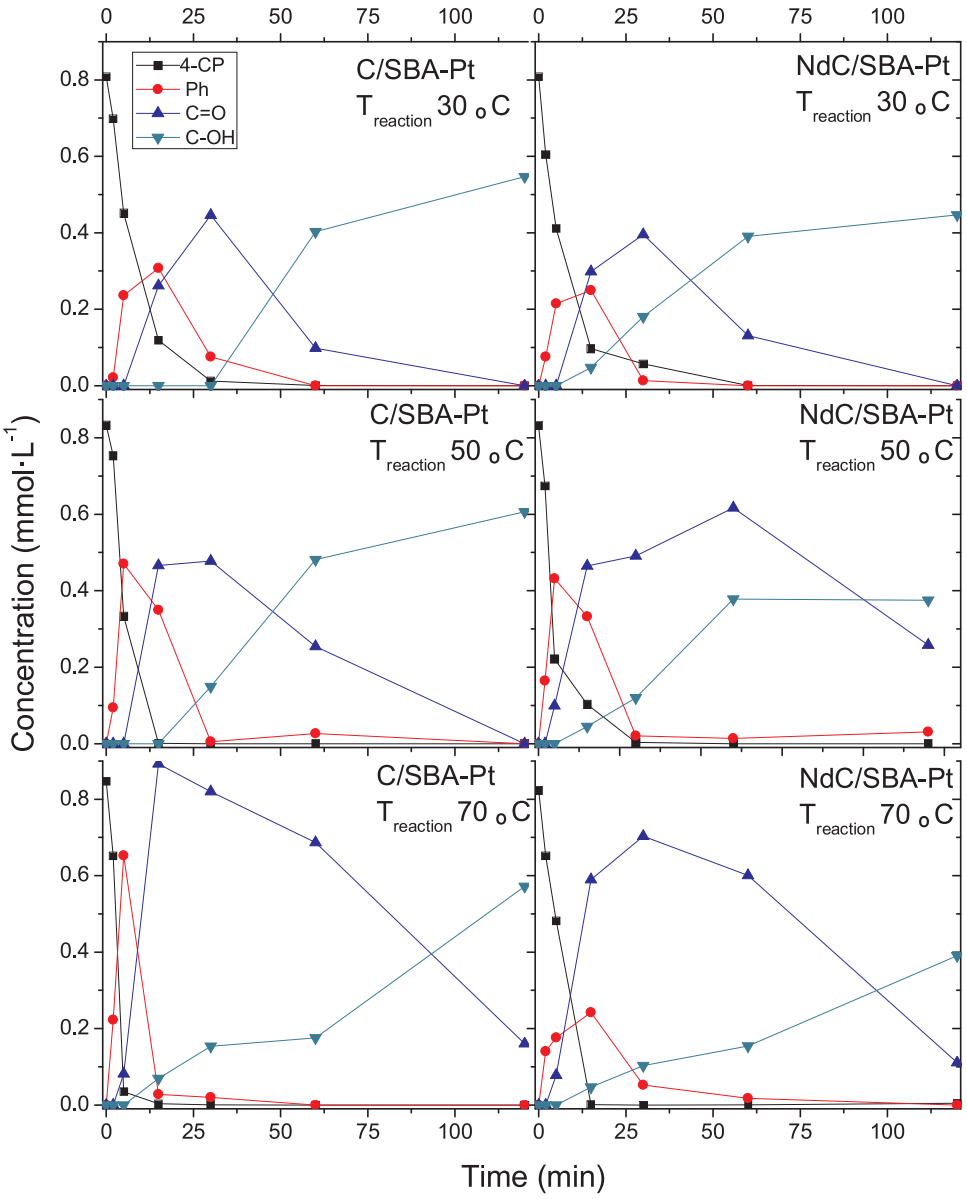

Fig. 9. Time course of 4-CP (■), phenol (●) and cyclohexanone (▲) and cyclohexanol (▼) concentration in the HDC experiments (30–70 °C, 5.8 mg Pt·L^{-1}).

Table 4
Selectivity and kinetic parameters obtained in the HDC runs with NdC/SBA-Pt and C/SBA-Pt catalysts at 30–70 °C (5.8 mg L^{-1}).

T (ºC)	Sample	Selectivity (%)[a]			k_{4CP}	R^2	activity (mmol·g^{-1} Pt·min^{-1})
		Ph	C = O	C-OH	(min^{-1})		
30	C/SBA-Pt	0	0	1.0	0.146	0.993	20
	NdC/SBA-Pt	0	0	1.0	0.120	0.970	17
50	C/SBA-Pt	0	0	1.0	0.190	0.900	27
	NdC/SBA-Pt	0	0.41	0.59	0.174	0.999	25
70	C/SBA-Pt	0	0.22	0.78	0.278	0.93	41
	NdC/SBA-Pt	0	0.22	0.78	0.352	0.95	50

[a] 120 min reaction time, 100% 4-CP conversion.

the support has a clear influence on the activity and selectivity, although this is not only related to the role of the support in the reaction but mostly to the growth of the metal phase on its surface.

A similar influence was observed for the selectivity (Fig. 10), with a higher production of cyclohexanone and cyclohexanol with NdC/SBAPt (IWI). The high hydrogenation activity is a common feature of the catalysts prepared in this work by incipient wetness impregnation and in situ colloidal synthesis and it is much higher than for the other catalysts in the aforementioned literature works. This behavior may be related to the high surface area, important contribution of mesoporosity and well interconnected pores of the nanostructured templated carbons used as supports in our case. It should also be noted that some traces of silica from the template may remain in the carbons and have some influence on the behavior of the catalysts. In this sense, Jin et al. [34] reported high activity for Pd catalysts supported on carbon silica composites, although hydrogenation of phenol was not observed.

4. Conclusions

Nanostructured carbon materials with different nitrogen content (0.15 and 1% w.) and equivalent morphology and porous texture have been obtained thanks to the application of the template method. The materials also have an ordered mesoporous structure with good connectivity. The anchorage of Pt NPs by incipient wet impregnation and by original in situ colloidal synthesis led to narrow NPs size distribution, although differences were found for the NPs prepared by incipient wetness impregnation on undoped and N-doped carbons, showing the role of the support in the growth of the Pt NPs.

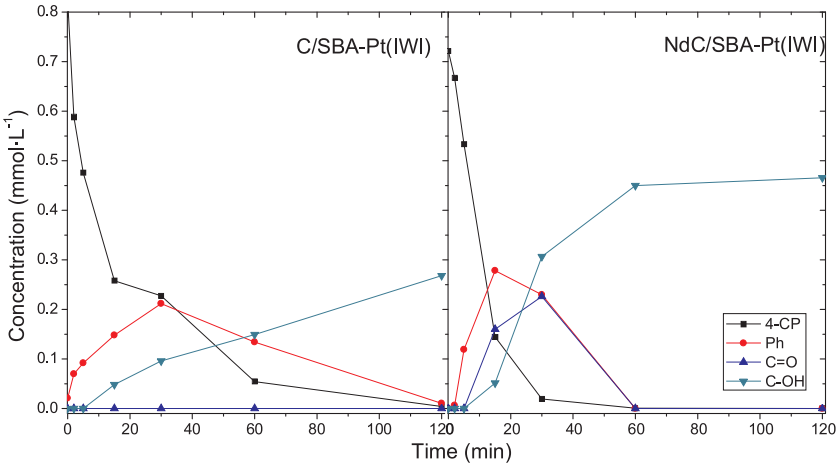

Fig. 10. Time course of 4-CP (■), phenol (●), cyclohexanone (▲) and cyclohexanol (▼) concentration for C/SBA-Pt(IWI) and NdC/SBA-Pt(IWI) catalysts (50 °C, 3.4 mg Pt·L^{-1}).

Table 5
Selectivity and kinetic parameters obtained in the HDC runs with C/SBA-Pt (IWI) and NdC/SBA-Pt(IWI) catalysts at 50 °C (3.4 mg Pt·L^{-1}).

Sample	Selectivity (%)[a]			k_{4CP} (min^{-1})	R^2	activity (mmol·g^{-1} Pt·min^{-1})
	Ph	C = O	C-OH			
C/SBA-Pt(IWI)	0	0	1.0	0.072	0.960	17
NdC/SBA-Pt(IWI)	0	0	1.0	0.119	0.997	25

[a] 120 min reaction time, 100% 4-CP conversion.

The catalysts showed a high hydrodechlorination activity as well as for further hydrogenation, which can be attributed to the unique structure of the support and maximizes the removal of toxicity. The activity was boosted by increasing the reaction temperature, especially in the case of the catalysts with N-doped support, indicating that intensification of the hydrodechlorination process with temperature can be better achieved for Pt catalysts using N-doped carbon supports. A low apparent activation energy was obtained for the disappearance of 4-CP, probably due to some contribution of adsorption and mass transfer to the overall rate.

The results for catalysts prepared by in situ colloidal synthesis showed a minor effect of support doping. On the contrary, for those prepared by incipient wetness impregnation an increase of activity was found when N-doped supports were used. These facts suggest that doping affects to the catalytic activity mostly through the way nanoparticles are grown on the support.

Acknowledgments

The authors also thank to Hexion Speciality Chemicals Iberica S.A. for providing the resol resin Bakelite®PF9934 FL. The authors thank financial support (CTQ2012-32821, CTQ2015-65491_R) and C. Ruiz-García for PhD grant (BES-2013-06608 5) to MINECO.

Appendix A. Supplementary data

Supplementary material related to this article can be found, in the online version, at doi:https://doi.org/10.1016/j.apcatb.2018.07.054.

References

[1] A. Sanchez-Sanchez, F. Suarez-Garcia, A. Martinez-Alonso, J.M.D. Tascon, Synthesis, characterization and dye removal capacities of N-doped mesoporous carbons, J. Colloid Interface Sci. 450 (2015) 91–100.
[2] X. Sheng, N. Daems, B. Geboes, M. Kurttepeli, S. Bals, T. Breugelmans, A. Hubin, I.F.J. Vankelecom, P.P. Pescarmona, N-doped ordered mesoporous carbons prepared by a two-step nanocasting strategy as highly active and selective electrocatalysts for the reduction of O-2 to H2O2, Appl. Catal. B-Environ. 176 (2015) 212–224.
[3] W. Zhang, F.S. Wang, X.L. Li, Y.S. Liu, J.T. Ma, Pd nanoparticles modified rod-like nitrogen-doped ordered mesoporous carbons for effective catalytic hydrodechlorination of chlorophenols, RSC Adv. 6 (2016) 27313–27319.
[4] B. Li, H. Nam, J. Zhao, J. Chang, N. Lingappan, F. Yao, T.H. Lee, Y.H. Lee, Nanoreactor of nickel-containing carbon–shells as oxygen reduction catalyst, Adv. Mater. 29 (2017) 1605083-n/a.
[5] L. Lan, Y. Liu, S. Liu, X. Ma, X. Li, Z. Dong, C. Xia, Effect of the supports on catalytic activity of Pd catalysts for liquid-phase hydrodechlorination/hydrogenation reaction, Environ. Technol. (2018) 1–9.
[6] W.A. Solomonsz, G.A. Rance, B.J. Harris, A.N. Khlobystov, Competitive hydrosilylation in carbon nanoreactors: probing the effect of nanoscale confinement on selectivity, Nanoscale 5 (2013) 12200–12205.
[7] S. Sadjadi, Organic Nanoreactors: From Molecular to Supramolecular Organic Compounds, (2016).
[8] B. Cornelio, A.R. Saunders, W.A. Solomonsz, M. Laronze-Cochard, A. Fontana, J. Sapi, A.N. Khlobystov, G.A. Rance, Palladium nanoparticles in catalytic carbon nanoreactors: the effect of confinement on Suzuki-Miyaura reactions, J. Mater. Chem. A Mater. Energy Sustain. 3 (2015) 3918–3927.
[9] J.P. Paraknowitsch, A. Thomas, Doping carbons beyond nitrogen: an overview of advanced heteroatom doped carbons with boron, sulphur and phosphorus for energy applications, Energy Environ. Sci. 6 (2013) 2839–2855.
[10] X.G. Duan, S. Indrawirawan, H.Q. Sun, S.B. Wang, Effects of nitrogen-, boron-, and phosphorus-doping or codoping on metal-free graphene catalysis, Catal. Today 249 (2015) 184–191.
[11] J. Lemus, J. Bedia, L. Calvo, I.L. Simakova, D.Y. Murzin, B.J.M. Etzold, J.J. Rodriguez, M.A. Gilarranz, Improved synthesis and hydrothermal stability of Pt/C catalysts based on size-controlled nanoparticles, Catal. Sci. Technol. 6 (2016) 5196–5206.
[12] J. Bedia, J. Lemus, L. Calvo, J.J. Rodriguez, M.A. Gilarranz, Effect of the operating conditions on the colloidal and microemulsion synthesis of Pt in aqueous phase, Colloids Surf. A 525 (2017) 77–84.
[13] J.A. Baeza, L. Calvo, M.A. Gilarranz, A.F. Mohedano, J.A. Casas, J.J. Rodriguez, Catalytic behavior of size-controlled palladium nanoparticles in the hydrodechlorination of 4-chlorophenol in aqueous phase, J. Catal. 293 (2012) 85–93.
[14] M.A. Keane, Supported transition metal catalysts for hydrodechlorination reactions, ChemCatChem 3 (2011) 800–821.
[15] C.D. Wagner, W.M. Riggs, L.E. Davis, J.F. Moulder, Handbook of x-ray Photoelectron Spectroscopy, Perkin-Elmer, 1979.
[16] E. Diaz, J.A. Casas, A.F. Mohedano, L. Calvo, M.A. Gilarranz, J.J. Rodriguez, Kinetics of 4-Chlorophenol hydrodechlorination with alumina and activated carbon-supported Pd and Rh catalysts, Ind. Eng. Chem. Res. 48 (2009) 3351–3358.
[17] M. Munoz, M. Kaspereit, B.J.M. Etzold, Deducing kinetic constants for the hydrodechlorination of 4-chlorophenol using high adsorption capacity catalysts, Chem. Eng. J. 285 (2016) 228–235.
[18] J. Rouquerol, F. Rouquerol, P. Llewellyn, G. Maurin, K.S.W. Sing, Adsorption by Powders and Porous Solids: Principles, Methodology and Applications, Second edition, (2013).
[19] V.K. Saini, M. Andrade, M.L. Pinto, A.P. Carvalho, J. Pires, How the adsorption properties get changed when going from SBA-15 to its CMK-3 carbon replica, Sep. Purif. Methods 75 (2010) 366–376.
[20] C.B. Molina, L. Calvo, M.A. Gilarranz, J.A. Casas, J.J. Rodriguez, Pd–Al pillared clays as catalysts for the hydrodechlorination of 4-chlorophenol in aqueous phase, J. Hazard. Mater. 172 (2009) 214–223.
[21] A.H. Pizarro, C.B. Molina, J.L.G. Fierro, J.J. Rodriguez, On the effect of Ce incorporation on pillared clay-supported Pt and Ir catalysts for aqueous-phase hydrodechlorination, Appl. Catal. B-Environ. 197 (2016) 236–243.
[22] M. Munoz, S. Ponce, G.-R. Zhang, B.J.M. Etzold, Size-controlled PtNi nanoparticles as highly efficient catalyst for hydrodechlorination reactions, Appl. Catal. B-Environ. 192 (2016) 1–7.
[23] E. Díaz, J.A. Casas, Á.F. Mohedano, L. Calvo, M.A. Gilarranz, J.J. Rodríguez,

Kinetics of the hydrodechlorination of 4-Chlorophenol in water using Pd, Pt, and Rh/Al2O3 catalysts, Ind. Eng. Chem. Res. 47 (2008) 3840–3846.
[24] L. Calvo, A.F. Mohedano, J.A. Casas, M.A. Gilarranz, J.J. Rodríguez, Treatment of chlorophenols-bearing wastewaters through hydrodechlorination using Pd/activated carbon catalysts, Carbon 42 (2004) 1377–1381.
[25] C.B. Molina, A.H. Pizarro, M.A. Gilarranz, J.A. Casas, J.J. Rodriguez, Hydrodechlorination of 4-chlorophenol in water using Rh-Al pillared clays, Chem. Eng. J. 160 (2010) 578–585.
[26] Y. Shindler, Y. Matatov-Meytal, M. Sheintuch, Wet hydrodechlorination of p-chlorophenol using Pd supported on an activated carbon cloth, Ind. Eng. Chem. Res. 40 (2001) 3301–3308.
[27] V. Felis, C. De Bellefon, P. Fouilloux, D. Schweich, Hydrodechlorination and hydrodearomatisation of monoaromatic chlorophenols into cyclohexanol on Ru/C catalysts applied to water depollution: influence of the basic solvent and kinetics of the reactions, Appl. Catal. B-Environ. 20 (1999) 91–100.
[28] G. Yuan, M.A. Keane, Liquid phase catalytic hydrodechlorination of chlorophenols at 273 K, Catal. Commun. 4 (2003) 195–201.
[29] Y. Liu, Z. Dong, X. Li, X. Le, W. Zhang, J. Ma, Aqueous-phase hydrodechlorination and further hydrogenation of chlorophenols to cyclohexanone in water over palladium nanoparticles modified dendritic mesoporous silica nanospheres catalyst, RSC Adv. 5 (2015) 20716–20723.
[30] M. Munoz, V. Kolb, A. Lamolda, Z.M. de Pedro, A. Modrow, B.J.M. Etzold, J.J. Rodriguez, J.A. Casas, Polymer-based spherical activated carbon as catalytic support for hydrodechlorination reactions, Appl. Catal. B-Environ. 218 (2017) 498–505.
[31] M. Munoz, G.-R. Zhang, B.J.M. Etzold, Exploring the role of the catalytic support sorption capacity on the hydrodechlorination kinetics by the use of carbide-derived carbons, Appl. Catal. B-Environ. 203 (2017) 591–598.
[32] P. Stathis, D. Stavroulaki, N. Kaika, K. Krommyda, G. Papadogianakis, Low trans-isomers formation in the aqueous-phase Pt/TPPTS-catalyzed partial hydrogenation of methyl esters of linseed oil, Appl. Catal. B-Environ. 209 (2017) 579–590.
[33] M. Zhou, H. Zhang, H. Ma, W. Ying, Kinetic modeling of acetic acid hydrogenation to ethanol over K-Modified PtSn catalyst supported on alumina, Ind. Eng. Chem. Res. 56 (2017) 8833–8842.
[34] Z. Jin, C. Yu, X. Wang, Y. Wan, D. Li, G. Lu, Hydrodechlorination of chlorophenols at low temperature on a novel Pd catalyst, Chem. Commun. (2009) 4438–4440.